Event-Driven Dynamic Platform Selection for Power-Aware Real-Time Anomaly Detection in Video

Calum G. Blair[1] and Neil M. Robertson[2]
[1]*Institute for Digital Communications, University of Edinburgh, Edinburgh, UK*
[2]*Visionlab, Heriot-Watt University, Edinburgh, UK*
c.blair@ed.ac.uk

Keywords: FPGA, GPU, Anomaly Detection, Object Detection, Algorithm Mapping.

Abstract: In surveillance and scene awareness applications using power-constrained or battery-powered equipment, performance characteristics of processing hardware must be considered. We describe a novel framework for moving processing platform selection from a single design-time choice to a continuous run-time one, greatly increasing flexibility and responsiveness. Using Histogram of Oriented Gradients (HOG) object detectors and Mixture of Gaussians (MoG) motion detectors running on 3 platforms (FPGA, GPU, CPU), we characterise processing time, power consumption and accuracy of each task. Using a dynamic anomaly measure based on contextual object behaviour, we reallocate these tasks between processors to provide faster, more accurate detections when an increased anomaly level is seen, and reduced power consumption in routine or static scenes. We compare power- and speed- optimised processing arrangements with automatic event-driven platform selection, showing the power and accuracy tradeoffs between each. Real-time performance is evaluated on a parked vehicle detection scenario using the i-LIDS dataset. Automatic selection is 10% more accurate than power-optimised selection, at the cost of 12W higher average power consumption in a desktop system.

1 INTRODUCTION

Opportunities for the use of advanced computer vision algorithms have increased to include surveillance and monitoring applications. We consider the deployment of such algorithms in a scenario with limited electrical power available for processing, such as surveillance from a mobile vehicle which may be running on battery power. Timely and accurate detections of objects and events are still important in such circumstances. Field Programmable Gate Arrays (FPGAs) and Graphics Processing Units (GPUs) offer large improvements in speed and power compared to a reference implementation on a standard CPU. This is increasingly relevant given the growing trend for smart cameras with processing capability, and the development of mobile general-purpose GPUs. Each algorithm implementation on one of these architectures will have its own performance characteristics — processing time, power consumption and algorithm accuracy — and will exist at a certain point in a multi-dimensional *design space*.

Using a heterogeneous system which contains *both* FPGAs and GPUs offers increased flexibility, allows decisions about the optimal platform to use to be moved from design time to run-time, and allows this decision to be updated in response to changing characteristics within the image or environment. In this paper, we use detection of parked vehicles in surveillance video as an anomaly detection application. First, we define an anomaly measure based on the motion of objects within a video. Using a heterogeneous system to process video, we select processing platforms — and hence alter system power, speed and accuracy characteristics — based on this anomaly level. We show how platform selection changes in response to changing anomaly levels, and compare the performance of this dynamically-mapped system against a static one optimised for power or speed. To summarise, the contributions of this work are: we describe our system consisting of multiple implementations of various object detection algorithms running across various accelerators in a heterogeneous hardware platform, demonstrate dynamic selection between these implementations in response to events within a scene, and describe the associated tradeoffs between power consumption and accuracy in a real-time system. This paper is laid out as follows: after describing relevant work in this section, §2 describes each algorithm used in the system and their perfor-

mance characteristics. Once an overall anomaly level is obtained, the mapping procedure described in §3 selects the next set of implementations. We discuss methodology in §4, results are presented in §5 and followed by analysis of the findings in §6. We conclude with pointers to future work in §7.

We consider first the architectural background of this work, and then place it in the context of other parked vehicle detection work evaluated on the same dataset. FPGAs and GPUs are two of the most common ways of improving performance of compute-intensive signal processing algorithms. In general, FPGAs offer a large speedup over reference implementations and draw low power because they instantiate logic which closely matches the application. However, their use of arbitrary-precision fixed-point arithmetic can impact accuracy slightly, and they require specialised knowledge to program, often incurring longer development times (Bacon et al., 2013). In contrast, GPUs have a software programming model, using large arrays of floating-point units to process data quickly, at the expense of power consumption. Their ubiquitous presence in PCs and laptops has made uptake very common in recent years, and the availability of Nvidia's CUDA language for both desktop and (in the near future) mobile and tablet devices greatly increases the potential for pervasive vision computing.

When building a system to perform a processing task, we consider each of the characteristics of FPGA and GPU and select the system which best suits our application, for example prioritising fast runtime over low power consumption. This has been done for various smaller algorithms, such as colour correction and 2-D convolution, as in (Cope et al., 2010). This design-time selection can also be done at a low level using an optimisation algorithm as shown by (Bouganis et al., 2009), although this is usually more concerned with FPGA area vs. latency trade-offs. As an example, Figure 1 shows design space exploration for power and time characteristics of implementation combinations used in this paper, with a well-defined Pareto curve at the left-hand side. To the authors' knowledge, little work has been done in the area of power-aware algorithm scheduling at runtime; the most appropriate is arguably (Yu and Prasanna, 2002), although this does not consider more than two performance characteristics or deal with changing optimisation priorities over time.

The UK Home Office supplies the i-LIDS dataset (Home Office Centre for Applied Science and Technology, 2011) used in §5, and this has been used for anomaly detection by other researchers. (Albiol et al., 2011) identify parked vehicles in this dataset's

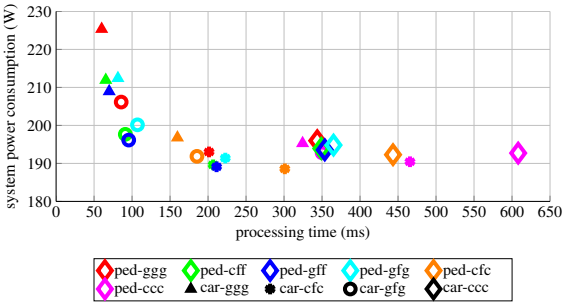

Figure 1: Design space exploration for power vs. time trade-offs for all possible combinations of car, pedestrian and motion detector implementations. Pedestrian implementations are labelled by colour, and car implementations by shape.

PV3 scenario with precision and recall of 0.98 and 0.96 respectively. However, their approach is considerably different from ours, in that they:- (a) require all restricted-parking lanes in the image to be manually labelled first, (b) only evaluate whether an object in a lane is part of the background or not, and (c) do not work in real-time or provide performance information. In addition, their P and R results do not denote events, but rather the total fraction of time during which the lane is obstructed. Due mainly to limitations within our detectors, our accuracy results alone do not improve upon this state-of-the-art, but given the points noted above, we are arguably trying to approach a different problem (anomaly detection under power and time constraints) than Albiol *et al.*

2 SYSTEM COMPONENTS

A flow diagram for the high-level frame processing framework is shown in Figure 2. It works on offline videos and dynamically calculates the number of frames to drop to obtain real-time performance at 25FPS. (We do not count video decode time or time for output image markup and display as part of processing time.) The 'detection algorithms' block generates bounding boxes with type information, which is used by the remaining algorithm stages. (An expanded version of this step showing all combinations is shown further on in Figure 4.) This section gives details of each algorithm in Table 1, *i.e.* the detection algorithms run on the image, and method for calculating image anomaly level. The object detectors and background subtractor were by far the most computationally expensive algorithm stages, so each of these had at least one accelerated version available. We use a platform containing a $2.4GHz$ dual-core Xeon CPU, a nVidia GeForce 560Ti GPU, and a Xilinx ML605

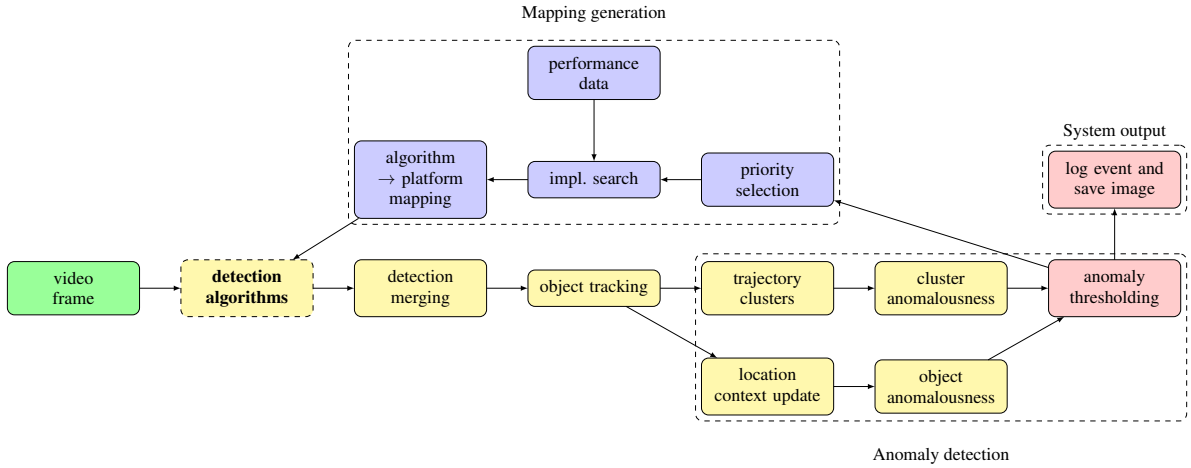

Figure 2: Frame processing and algorithm mapping loop in anomaly detection system.

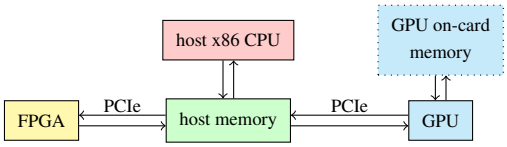

Figure 3: Arrangement of accelerated processors within heterogeneous system. Each processor can access host main memory over PCI express, and the two accelerators have private access to on-card memory.

Table 1: Algorithms and implementations used in the system.

Algorithm	Implementation(s)		
Ped. Detection: HOG (§2.1)	FPGA	GPU	CPU
Car Detection: HOG (§2.2)	FPGA	GPU	CPU
Motion Segment: MoG (§2.3)		GPU	
Tracking: Kalman Filter (§2.5)			CPU
Trajectory Clustering (§2.6)			CPU
Bayesian Motion Context (§2.7)			CPU

board with a XC6VLX240T FPGA, as shown in Figure 3. Implementation performance characteristics are shown in Table 2 where appropriate.

2.1 Pedestrian Detection with HOG

We use various accelerated versions of the Histograms of Oriented Gradients pedestrian detector described in (Dalal and Triggs, 2005); this algorithm is

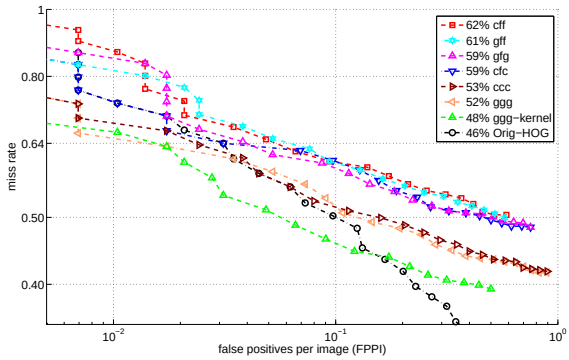

Figure 5: DET curve (False positives per image against miss rate) for HOG pedestrian detector.

well-understood and has been characterised on various platforms. Each version is split into three computationally expensive parts (image resizing, histogram generation and support vector machine (SVM) classification), and these are implemented across different processing platforms (FPGA, GPU and CPU) as described by (Blair et al., 2013). These mappings are shown in the left hand side of Figure 4. The following mnemonics are used in this Figure and elsewhere: a single implementation is referred to by the architecture each part runs on, *e.g.* running HOG with resizing on CPU, histogram generation on FPGA and classification on CPU is *cfc*. Each implementation has different power consumption, speed and accuracy characteristics, summarised in Table 2. These could be switched between dynamically at runtime with no performance penalty. We show a False Positives Per Image (FPPI) curve for each implementation in Figure 5. Detector errors (*e.g.* in Figure 6) affect overall accuracy dramatically. Errors in the training phase

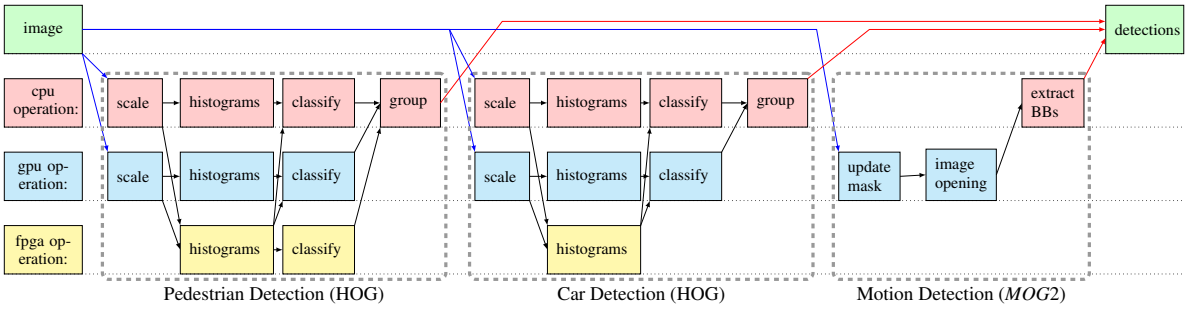

Figure 4: All possible mappings of image processing algorithms to hardware. Multiple possible implementation steps within one algorithm are referred to by the platform they run on. Running HOG with a resize step on GPU, histograms on FPGA and classification on GPU is referred to throughout as *gfg*. Data transfer steps not shown.

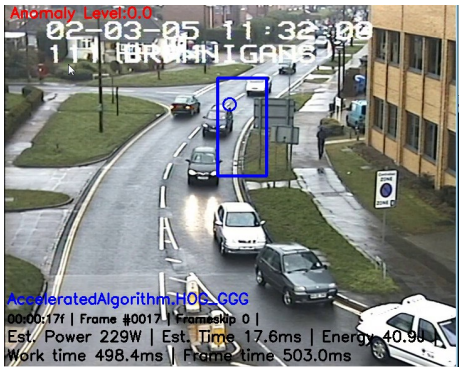

Figure 6: False positives (blue rectangle representing pedestrian) from object detectors affected training and testing performance, both directly and through learned context measures.

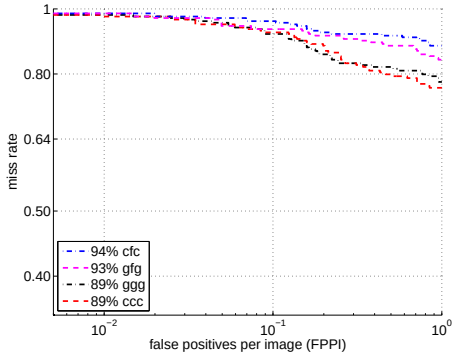

Figure 7: DET curve for HOG car detector.

also affect the clusters and context heatmaps in §2.6 and §2.7.

2.2 Car Detection with HOG

The HOG algorithm was again selected for car detection due to the presence of existing implementations running in near-realtime across multiple architectures. The CPU and GPU implementations of HOG on OpenCV were modified to use the parameters in (Dalal, 2006) for car detection. A FPGA version was also implemented by modifying the *cfc* and *gfg* versions in (Blair et al., 2013).

These implementations were trained on data from the 2012 Pascal Visual Object Classes Challenge (Everingham et al., 2009). The SVM was learned as described in (Dalal and Triggs, 2005). An FPPI curve is in Figure 7, generated from all positive images in Pascal-VOC at scale factor 1.05. This shows HOG-CAR is not as accurate as the pedestrian version; this is probably due to the smaller dataset and wider variation in training data. The detector is only trained on cars, although during testing it was also possible to detect vans and trucks. All designs (pedestrian HOG with histogram and window outputs, and car HOG with histogram outputs) were implemented on the same FPGA, with detectors running at $160MHz$. Overall resource use was 52%.

2.3 Background Subtraction with MOG

The Mixture of Gaussians (MOG) algorithm was used to perform background subtraction and leave foreground objects. The OpenCV GPU version uses Zivkovic's implementation (Zivkovic, 2004). Contour detection was performed to generate bounding boxes as shown in Figure 8(a). As every bounding box was passed to one or more computationally expensive algorithms, early identification and removal of overlaps led to significant reductions in processing time. Bounding boxes with $\geq 90\%$ intersection were compared and the smaller one was discarded; *i.e.* we discard B_i if:

$$\frac{B_i \cap B_j}{area(B_j)} \geq 0.9 \;\&\; area(B_i) < area(B_j)\,. \quad (1)$$

Occasionally heavy camera shake, fast adjustment of the camera gain, or fast changes in lighting conditions

(a) Motion detection by background subtraction in video.

(b) False motion regions from camera shake and illumination changes.

Figure 8: Bounding box extraction from Mixture-of-Gaussians GPU implementation.

would cause large portions of the frame to be falsely indicated to contain motion, as shown in Figure 8(b). When this occurred, all bounding boxes for that frame were treated as unreliable and discarded.

2.4 Detection Merging

Object detections were generated from two sources: a direct pass over the frame by HOG, or by detections on a magnified region of interest triggered by the background subtractor. Motion regions were extracted, magnified by 1.5× then passed to both HOG versions. This allowed detection of objects smaller than the minimum window size. Candidate detections from global and motion-cued sources were filtered using the 'overlap' criterion from the Pascal VOC challenge (Everingham et al., 2009): $a_0 = area(B_i \cap B_j)/area(B_i \cup B_j)$. Duplicates were removed if the two object classes were compatible and $a_0(B_i, B_j) > 0.45$. Regions with unclassified motion were still passed to the tracker matcher to allow identification of new tracks or updates of previously-classified detections.

2.5 Object Tracking

A constant-velocity Kalman filter was used to smooth all detections. These were projected onto a ground plane before smoothing, as shown in Figure 9.

As trajectory smoothing and detection matching operate on the level of abstraction of objects rather than pixels or features, the number of elements to process is low enough, and the computations for each one are simple enough that this step is not considered as a candidate for parallelization.

2.6 Trajectory Clustering

The trajectory clustering algorithm used is a reimplementation of that described by (Piciarelli and Foresti, 2006), used for detection of anomalies in traffic

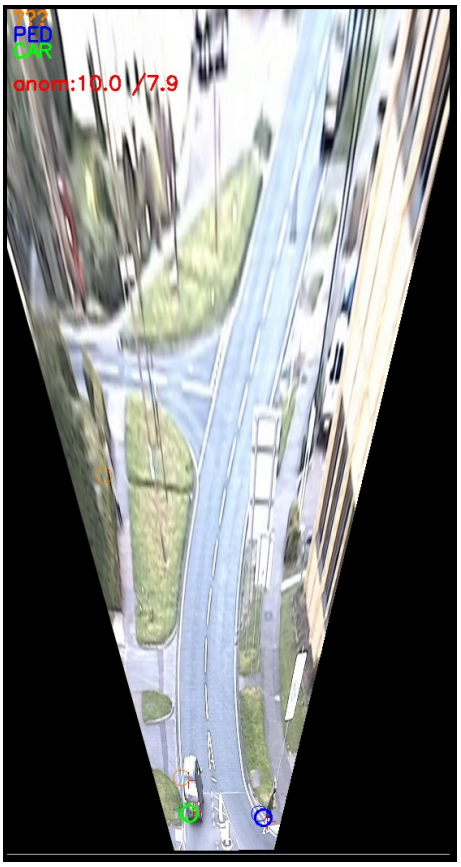

Figure 9: Object tracking on an image transformed onto the base plane. Green, blue and orange circles represent car, pedestrian and undetermined (motion-only) clusters respectively.

flow. The authors apply the algorithm to fast-moving motorway traffic, whereas the i-LIDS scenes have more object classes (pedestrians and vehicles), several scene entrances and exits, greater opportunities for occlusion, and long periods where objects stop moving and start to be considered part of the background. Starting with a trajectory $T_i = (t_0, t_1, \ldots, t_n)$ consisting of smoothed detections over several frames, we match these to and subsequently update a set of clusters. Each cluster C_i contains a vector of elements c_j each with a point x_j, y_j and a variance σ_j. Clusters are arranged in trees, with each having zero or more children. One tree (starting with a *root cluster*) thus describes a single point of entry to the scene and all observed paths taken through the scene from that point. For a new (unmatched) trajectory T_u, all root clusters and their children are searched to a given depth and T_u is assigned to the closest C if a Euclidean distance measure d is below a threshold. If T_u does not match anywhere, a new root cluster is created. For T previously matched to a cluster, clusters can be extended,

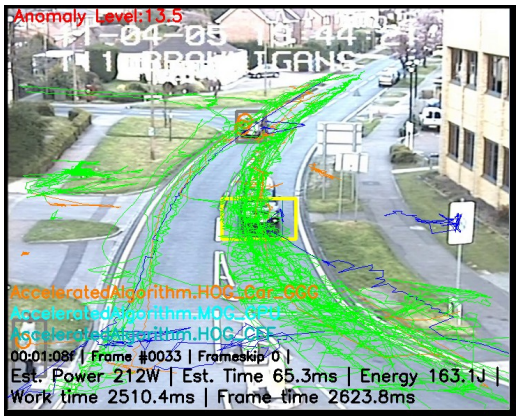

Figure 10: Trajectory clustering via learned object clusters, re-projected onto camera plane. Green, blue and orange tracks represent cars, pedestrians and undetermined (motion-only) objects respectively.

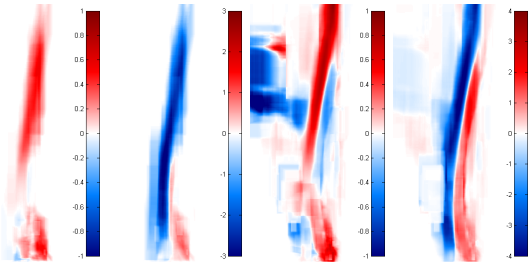

(a) $v_{x,ped}$ (b) $v_{y,ped}$ (c) $v_{x,car}$ (d) $v_{y,car}$

Figure 11: Ground-plane motion intensity maps built using movement from different object classes in PV3. In (d), on-road vertical motion away from (blue) and toward the camera (red) is distinct and clearly defined. Velocity scale is in pixels per frame.

points updated or new child clusters split off as new points are added to T. As with §2.4, clustering operates on a relatively small number of objects and is not computationally expensive, so was not considered for acceleration. Learned class-specific object clusters are shown in Figure 10, projected back onto the camera plane.

2.7 Contextual Knowledge

Contextual knowledge relies on known information about the normal or most common actions within the scene (Robertson and Letham, 2012). Position and motion information can capture various examples of anomalous behaviour: for example stationary objects in an unusual location, or vehicles moving the wrong way down a street. Unsupervised learning based on the output of the object classifiers during training sequences was used to learn scene context.

Type-specific information about object presence at different locations in the base plane was captured by recording the per-pixel location of each base-transformed bounding box. Average per-pixel velocity $\bar{v}$ in $x-$ and $y-$directions was obtained from the object trackers. For an object at base plane location $(x\ldots x',\ y\ldots y')$ with $x-$velocity v_x and update rate $\alpha = 0.0002$,

$$\bar{v}_{(x\ldots x',\ y\ldots y')} = (1-\alpha)\bar{v}_{(x\ldots x',\ y\ldots y')} + \alpha v\,. \qquad (2)$$

This is shown in Figure 11. For most conceivable traffic actions, presence and motion information is appropriate; however, this fails to capture more complex interactions between people. We therefore focus on behaviour involving vehicles.

2.8 Anomaly Detection

Based on §2.7 and §2.6 we can define an anomalous object as one which is present in an unexpected area, or one which is present in an expected area but moves in an unexpected direction or at an unexpected speed. A Bayesian framework is used to determine if an object's velocity in the x and y directions should be considered anomalous, based on the difference between it and the known average velocity $\bar{v}$ in that region. We define the probability of an anomaly at a given pixel $p(A|D)$, given detection of an object at that pixel:

$$p(A|D) = \frac{p(D|A)p(A)}{p(D|A)p(A) + p(D|\bar{A})p(\bar{A})}\,, \qquad (3)$$

where the prior probability of an anomaly anywhere in the image, $p(A)$, is set to a constant value. $p(D|A)$, the likelihood of detecting an event at any pixel in the presence of an anomaly, is constant (*i.e.* we assume that an anomaly can occur with equal probability anywhere within the image), and $p(\bar{A}) = 1 - p(A)$.

$p(D|\bar{A})$ is a measure based on the learned values for $\bar{v}_x$ or $\bar{v}_y$. It expresses the similarity of the observed motion to mean motion at that pixel, and returns values between $(0.01, 0.99)$. These are based on the distance between, and relative magnitudes of, v and $\bar{v}$:

$$d_v = \begin{cases} sgn(\bar{v})\max(C|\bar{v}|, |\bar{v}| + C), & \text{if } sgn(\bar{v}) \\ & == sgn(v) \\ & \&|v| > |\bar{v}| \\ sgn(\bar{v})\min(-|\bar{v}|/2, |\bar{v}| - c), & \text{otherwise.} \end{cases} \qquad (4)$$

Here, C and c are forward and reverse-directional constants. d_v is then used to obtain a linear equation for v, with a gradient of $a = (0.01 - 0.99)/(d_v - \bar{v})$. Finally, b is obtained in a similar manner, and v is projected onto this line to obtain a per-pixel likelihood that v is *not* anomalous:

$$y = av + b\,, \qquad (5)$$

$$p(D|\bar{A}) = \max(0.01, \min(0.99, y))\,. \qquad (6)$$

Equation 3 now gives an object anomaly measure UO_x. This is repeated for $y-$velocity data to obtain UO_y.

This is combined with UC, an abnormality measure for the cluster linked to that object. When a trajectory moves from one cluster to one of its children, leaves the field of view, or is lost, the number of transits through that cluster is incremented. For any trajectory T matched to a cluster C_p with children C_{c1} and C_{c2}, the number of trajectory transitions between C_p and all C_c is also logged, updating a frequency distribution between C_{c1} and C_{c2}. These two metrics (cluster transits and frequency distributions of parent–to–child trajectory transitions) allow anomalous trajectories to be identified. If C_i is a root node, $UC(C_i) = (1+transits(C_i))^{-1}$. Otherwise if C_i is one of n child nodes of C_p,

$$UC(C_i) = 1 - \frac{transitions(C_p \rightarrow C_i)}{\sum_{j=1}^{n} (transitions(C_p \rightarrow C_j))}. \quad (7)$$

An overall anomaly measure U_i for an object i with age τ is then obtained:

$$U_i = w_o \frac{\Sigma_1^{\tau_i} UO_x}{\tau_i} + w_o \frac{\Sigma_1^{\tau_i} UO_y}{\tau_i} + w_c UC_i, \quad (8)$$

and U_{max} is updated via $U_{max} = \max(U_{max}, U_i)$. The UO measures are running averages over τ. An object has to appear as anomalous for a time threshold t_A before affecting U_{max}. All w are set to 10, with the anomaly detection threshold set at 15; two detectors are thus required to register an object as anomalous before it is logged.

3 DYNAMIC MAPPING

The mapping mechanism selects algorithm implementations used to process the next frame. This runs every time a frame is processed, allowing selection of a new set of implementations M in response to changing scene characteristics. M can be any combination of paths through the algorithms in Figure 4; Figure 1 shows system power vs. time for all such combinations. Ten credits are allocated between the three priorities P used to influence the selection of M: power consumption w_p, processing time w_t and detection accuracy w_ε. Here we assume that a higher level of anomaly in the scene should be responded to with increased processing resources to obtain more information about the scene in a timely fashion, with fewer dropped frames, and at the expense of lower power consumption. Conversely, frames with low or zero anomaly levels cause power consumption to be scaled back, at the expense of accuracy and processing time. Realtime processing is then maintained by dropping a greater number of frames. Prioritisation could be either manual or automatic. When automatic prioritisation was used, (*i.e.* the system was allowed to respond to scene events by changing its mapping) the *speed* priority was increased to maximum when $U_{max} \geq 15$. A level of hysteresis was built in by maximising the *power* priority when $U_{max} < 12$. After every processed frame, if $t_{process} > FPS^{-1}$, then $\lceil t_{process} \times FPS \rceil$ frames are skipped to regain a realtime rate.

Table 2: Performance characteristics (Processing Time (ms), System Power (W) and Detection Accuracy (log-average miss rate (%))) for various algorithm implementations on 770×578 video. Baseline power consumption was $147W$.

Algo.	Impl.	Time (ms)	Power (W)	Accuracy (%)
HOG (PED)	*ggg*	17.6	229	52
	cff	23.0	190	62
	gff	27.5	186	61
	gfg	39.0	200	59
	cfc	117.3	187	59
	ccc	282.0	191	53
HOG (CAR)	*ggg*	34.3	229	89
	cfc	175.6	189	94
	gfg	60.0	200	92
	ccc	318.0	194	89
MOG	GPU	8.1	202	N/A

Once a list of candidate algorithms (HOG-PED, HOG-CAR and MOG) and a set of performance priorities is generated, implementation mapping is run. This uses performance data for each algorithm implementation, shown individually for all algorithms in Table 2. Exhaustive search is used to generate and evaluate all possible mappings, with a cost function:

$$C_i = w_p P_i + w_t t_i + w_\varepsilon \varepsilon_i, \quad (9)$$

where all w are controlled by P. Estimated power, runtime and accuracy is also generated at this point. The lowest-cost mapped algorithms are then run sequentially to process the next frame and generate detections.

4 EVALUATION METHODS

Clusters and heatmaps were initialised by training on two 20-minute daylight clips from the i-LIDS training set. Each test sequence was then processed in approximately real time using this data. Clusters and heatmaps were not updated between test videos. The

homography matrices used to register each video onto the base plane were obtained manually. Tests were run three times and referred to as follows, using the prioritisation settings described in §3:

speed speed prioritised, auto prioritisation off;
power power prioritised, auto prioritisation off;
auto anomaly-controlled auto prioritisation on.

For each run, all anomalous events (defined as objects having $U > 15$ for more than a fixed time limit $t_A = 10$ or 15 seconds) were logged and compared with ground-truth data. Power consumption for one frame was estimated by averaging the energy used to process each implementation over runtime for that frame. Average power consumption over a sequence of frames was obtained in the same manner.

A modified version of the i-LIDS criteria was used to evaluate detection performance. Events count as true positives if they are registered within 10 seconds of the start of an event. For parked vehicles, i-LIDS considers the start of the event to be one full minute *after* the vehicle is parked, whereas we consider the start of the event to be when it parks. We may thus flag events *before* the timestamp given in the ground truth data. The time window for matching detections is thus 70 or 75 seconds long. The i-LIDS criteria only require a binary alarm signal in the presence of an anomaly; however, we require anomalous tracks to be localised to the object causing the anomaly. The detection in Figure 12(d) is thus incorrect; the white van is stopped and should be registered as an anomaly, but the car on the left is flagged instead. This counts as one false-negative and one false-positive event.

Table 3: Detection performance (precision and recall) for parked vehicle events on i-LIDS PV3. F_1-scores are shown for operational awareness (OA) and event logging (EL).

Priority	p	r	$F_{1,OA}$	$F_{1,ER}$
for $t_A = 10$ seconds				
power	0.083	0.133	0.0957	0.1317
speed	0.105	0.194	0.1254	0.1913
auto	0.102	0.194	0.1226	0.1912
for $t_A = 10$ seconds, daylight only				
power	0.121	0.148	0.1294	0.1475
speed	0.130	0.214	0.1510	0.2118
auto	0.125	0.214	0.1466	0.2115
for $t_A = 15$ seconds				
power	0.118	0.065	0.0910	0.0652
speed	0.381	0.258	0.3259	0.2594
auto	0.222	0.133	0.1797	0.1342
for $t_A = 15$ seconds, daylight only				
power	0.167	0.065	0.1067	0.0652
speed	0.500	0.258	0.3752	0.2601
auto	0.286	0.133	0.2030	0.1345

Table 4: Processing performance for all prioritisation modes, showing percentage of frames skipped, ($fskip$), processing time including (t_{frame}) and excluding overheads (t_{work}) compared to source frame time (t_{src}), and mean estimated power above baseline (P^*_{work}). Idle/baseline power is $147W$.

Priority	$fskip$ (%)	t_{frame}/t_{src} (%)	t_{work}/t_{src} (%)	P^*_{work} (W)
power	75.8	125.4	87.9	49.1
speed	59.5	124.3	81.7	72.8
auto	66.5	127.8	83.4	61.9
daylight only				
power	75.5	125.4	87.9	49.1
speed	60.1	124.2	82.0	78.4
auto	66.0	122.0	83.4	61.8

5 RESULTS

i-LIDS uses the F_1 score ($F_1 = (\alpha+1)rp/(r+\alpha p)$) for comparing detection performance. α is set at 0.55 for real-time operational awareness (to reduce false-alarm rate), or 60 for event logging (to allow logging of almost everything with low precision).

Table 3 shows precision, recall and F_1 scores for all "parked vehicle" events in the PV3 scenario for $t_A = 10$ and 15 seconds. Night-time sequences have no events but still generate a large proportion of false positives, so this also shows results for daylight-only ("day" and "dusk" clips) separately.

Table 4 shows performance details for all three priority modes. The t_{frame} column shows overall execution time (including overheads) relative to total source video length. The processing time column does not include overheads. It assumes that a raw video frame is already present in memory, and frame-by-frame video output is not required (*i.e.* only events are logged). In this case, the system runs faster than realtime, with the percentage of skipped frames shown in the $fskip$ column. The slower power-optimised priority setting causes more frames to be skipped.

Figure 12 shows example detections logged after t_A seconds. While some true positives are detected (up to 50% in the best case), many false negatives and false positives are present, and have various causes. False positive are often caused by the background subtractor erroneously identifying patches of road as foreground, caused by the need to acquire slow-moving or waiting traffic in the same region. False negatives are, in general, caused by poor performance of the object classifiers or background subtractor. Directly failing to detect partially occluded ob-

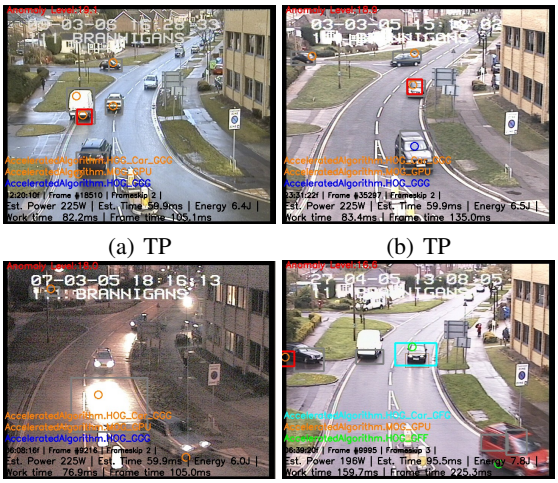

(a) TP (b) TP

(c) FN (d) FN, FP

Figure 12: True detections and failure modes of anomaly detector on i-LIDS PV3. (a), (b): true positives in varying locations. (c): false negative caused by occlusion. (d) is treated as a false negative and a false positive as the detector identifies the car on the left instead of the van parked beside it.

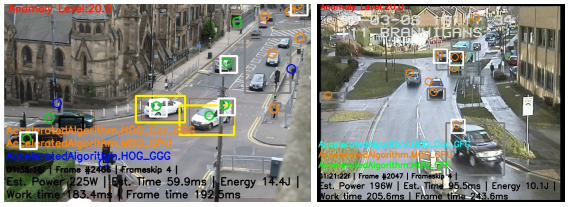

(a) High-quality video (b) i-LIDS video

Figure 13: Dataset quality impacts quality of detections: in a separate video (a), video quality allows classification of most objects as either pedestrian (blue circle) or car (green circle). In i-LIDS, (b), detections often remain as uncategorised motion (orange circle).

jects (as in Figure 12(c)), or stationary, repeated false detections in regions overlapping the roadside which are generated during training can both cause anomalies to be missed. Poorer video quality also reduces detection accuracy, as shown in Figure 13.

6 DISCUSSION

Given that the system must run in real-time (as we drop frames to ensure a close-to-realtime rate), the main tradeoffs available here are accuracy and power; optimising for time allows more frames to be processed, which in combination with the natural increased detection accuracy of the *ggg* detectors, increases p and r. This is borne out by the data in Table 3.

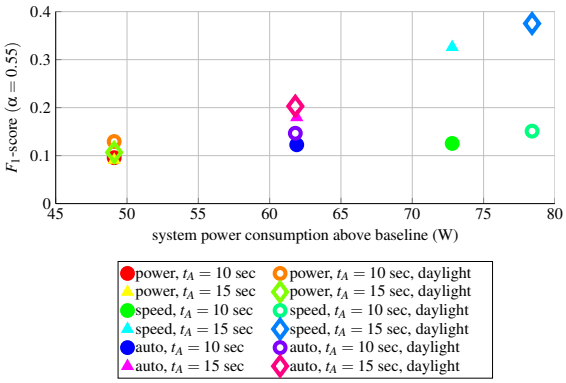

Figure 14: F_1-scores for operational awareness ($\alpha = 0.55$) against power consumption, for various time thresholds.

The key figures in Table 4 are mean estimated power consumption above baseline; there is $29W$ range in average power consumption between highest-power and lowest-power priority settings. When the system was run with speed prioritised with the FPGA turned off, power consumption was $208W$, or $62W$ above baseline. The average power for auto-prioritised mode with the FPGA on was $61.9W$, but this is dependent on the dataset used; datasets with fewer moving objects would have a lower average power consumption than this. As Figure 14 shows, running the system in automatic prioritisation mode allows an increase in accuracy of 10% over the lowest-power option for a cost of $12W$ in average power consumption. A further 17% gain in F_1-score (from *auto* to *speed*) costs an extra $17W$ above baseline. These results show a clear relationship between power consumption and overall detection accuracy.

6.1 Comparison to State-of-the-Art

Some previous work has considered four clips made publicly available from i-LIDS, known as AVSS and containing 4 parked-vehicle events, classed as easy, medium, hard and night. The only work we are aware of which evaluates the complete i-LIDS dataset is (Albiol et al., 2011). Using spatiotemporal maps and manually-applied lane masks per-clip to denote areas in which detections are allowed, Albiol *et al*. are able to improve significantly on the precision and recall figures given above, reaching $p-$ and $r-$values of 1.0 for several clips in PV3. They do not provide performance information but note that they downscale the images to 240×320 to decrease evaluation time. In their work they discuss the applicability and limitations of background subtractors for detecting slow-moving and stopped objects, as well as discussing the same difficulties with the i-LIDS data previously

seen in Figure 13. As in §1, we also consider real-time implementation and power consumption, with an end goal of a fully automatic system. Unlike Albiol *et al*.'s requirement for manual operator intervention, we only need to re-register videos between clips to overcome camera movement, which could be done automatically. If we only consider our detector accuracy compared to those of other researchers working on this data, we cannot improve upon existing results. However, we are tackling the novel problem of power-aware anomaly detection rather than offline lane masking, and any accuracy measurement must be traded against other characteristics, as Figure 14 shows. The most obvious way to improve these results would be to use the currently best-performing object classifiers, but implementing multiple heterogeneous versions of these would take prohibitively long to develop.

7 CONCLUSION

We have described a real-time system for performing power-aware anomaly detection in video, and applied it to the problem of parked vehicle detection. We are able to select between various algorithm implementations based on the overall object anomaly level seen in the image, and update this selection every frame. Doing this allows us to dynamically trade off power consumption against detection accuracy, and shows benefits when compared to fixed power- and speed-optimised versions. Although the accuracy of our detection algorithms (HOG) alone is no longer state-of-the-art, future improvements include introduction of more advanced object classifiers (such as (Benenson and Mathias, 2012)) and a move to a mobile chipset, which would reduce idle power consumption while maintaining both speed and accuracy, with the trade-off of increased development time.

ACKNOWLEDGEMENTS

We gratefully acknowledge the work done by Scott Robson at Thales Optronics for his FPGA implementation of the histogram generator for the CAR-HOG detector.
This work was supported by the Institute for System Level Integration, Thales Optronics, the Engineering and Physical Sciences Research Council (EPSRC) Grant number EP/J015180/1 and the MOD University Defence Research Collaboration in Signal Processing.

REFERENCES

Albiol, A., Sanchis, L., Albiol, A., and Mossi, J. M. (2011). Detection of Parked Vehicles Using Spatiotemporal Maps. *IEEE Transactions on Intelligent Transportation Systems*, 12(4):1277–1291.

Bacon, D., Rabbah, R., and Shukla, S. (2013). FPGA Programming for the Masses. *Queue*, 11(2):40.

Benenson, R. and Mathias, M. (2012). Pedestrian detection at 100 frames per second. In *Computer Vision and Pattern Recognition (CVPR), 2012 IEEE Conference on*, pages 2903–2910.

Blair, C., Robertson, N. M., and Hume, D. (2013). Characterising a Heterogeneous System for Person Detection in Video using Histograms of Oriented Gradients: Power vs. Speed vs. Accuracy. *IEEE Journal on Emerging and Selected Topics in Circuits and Systems*, 3(2):236–247.

Bouganis, C.-S., Park, S.-B., Constantinides, G. A., and Cheung, P. Y. K. (2009). Synthesis and Optimization of 2D Filter Designs for Heterogeneous FPGAs. *ACM Transactions on Reconfigurable Technology and Systems*, 1(4):1–28.

Cope, B., Cheung, P. Y., Luk, W., and Howes, L. (2010). Performance Comparison of Graphics Processors to Reconfigurable Logic: A Case Study. *IEEE Transactions on Computers*, 59(4):433–448.

Dalal, N. (2006). *Finding People in Images and Videos*. PhD Thesis, Institut National Polytechnique de Grenoble / INRIA Grenoble.

Dalal, N. and Triggs, B. (2005). Histograms of oriented gradients for human detection. In *Computer Vision and Pattern Recognition, 2005. CVPR 2005.*, pages 886– 893. IEEE Computer Society.

Everingham, M., Gool, L., Williams, C. K. I., Winn, J., and Zisserman, A. (2009). The Pascal Visual Object Classes (VOC) Challenge. *International Journal of Computer Vision*, 88(2):303–338.

Home Office Centre for Applied Science and Technology (2011). *Imagery Library for Intelligent Detection Systems (I-LIDS) User Guide*. UK Home Office, 4.9 edition.

Piciarelli, C. and Foresti, G. (2006). On-line trajectory clustering for anomalous events detection. *Pattern Recognition Letters*, 27(15):1835–1842.

Robertson, N. and Letham, J. (2012). Contextual Person Detection in Outdoor Scenes. In *Proc. European Conference on Signal Processing (EUSIPCO 2012)*.

Yu, Y. and Prasanna, V. (2002). Power-aware resource allocation for independent tasks in heterogeneous real-time systems. In *Ninth International Conference on Parallel and Distributed Systems, 2002. Proceedings.*, pages 341–348. IEEE Comput. Soc.

Zivkovic, Z. (2004). Improved adaptive Gaussian mixture model for background subtraction. In *Proceedings of the 17th International Conference on Pattern Recognition, 2004. ICPR 2004.*, volume 2, pages 28–31. IEEE.